J. Fluid Mech. (1997), *vol.* 337, *pp.* 283–301

The evolution of initially turbulent bluff-body wakes at high internal Froude number

By G. R. SPEDDING

Department of Aerospace Engineering, University of Southern California, Los Angeles, CA 90089-1191, USA

(Received 5 June 1996 and in revised form 15 October 1996)

Coherent vortex structures are formed in the late wakes of towed spheres for all values of the internal Froude number, $F \equiv 2U/ND \in [10, 240]$ (U is the body speed, D its diameter, and N is the buoyancy frequency). The eventual emergence of the long-lived and stable pattern of alternating-signed patches of vertical vorticity is characteristic of all towed-sphere wakes, from those dominated by internal lee waves at $F = 1$, to initially fully turbulent early wakes at $F \geqslant 4$. At late times, the local Froude number is always low, and a characteristic stratified wake structure and dynamics result. These wakes have high mean wake defect velocities compared with non-stratified wakes, but the decay rates of energy and enstrophy are similar. Experimental evidence is presented for the existence of an intermediate non-equilibrium (NEQ) regime with very low decay rates of kinetic energy, that precedes the late wake. The NEQ regime is the period when the initial turbulence reorganizes under the increasingly (relative to the decaying turbulent kinetic energy) powerful influence of the background density gradient, accompanied by conversion of potential to kinetic energy as the wake turbulence collapses. The stable long-lived late-wake structure that eventually emerges has a high degree of order and coherence that reflects the initial wake instability. A universal curve for the energy decay of all stratified drag wakes at high Froude and Reynolds numbers is proposed.

1. Introduction

1.1. *Previous work*

The evolution of the turbulent wake of a towed sphere in a stable background density gradient is a convenient experimental model for investigating fundamental problems in the decay of isolated patches of turbulence in stratified oceans or atmospheres, or in application to more practical problems of turbulent wake generation and detection for slender bodies of various kinds. The competition between inertial and buoyancy forces is expressed numerically by the internal Froude number, $F \equiv 2U/ND$ (the buoyancy, or Brunt–Väisälä frequency, N, is defined here as $N^2 = -(g/\rho_0)(\partial\rho/\partial z)$). In many applications, both Reynolds and Froude numbers can be very large initially, but in decaying flows that originate in intermittent bursts of activity, the local Froude number will eventually become of order one and the motions are strongly constrained by the ambient stratification. These flows can be termed quasi-two-dimensional, in that the vertical velocity component (w in z, opposed by the local gravitational restoring force) is very small compared with the horizontal components, but at the same time, the flow is not assumed to be uniform in z. Lighthill (1996) shows how

residual time-invariant motions emerge from small initial disturbances to uniformly stratified fluids, and Pearson & Linden (1983) describe the almost-horizontal modes of motion in the final stages of decay of turbulence in a stable stratification. When the initial conditions are fully turbulent, the transition between a disorganized three-dimensional flow and the final bouyancy-dominated state has not yielded to simple analysis.

The most broad overview of stratified turbulent wake flows, encompassing many applications, remains that of Lin & Pao (1979). Since then, a variety of experimental techniques has recently been brought to bear on the problem, and the basic phenomenology of the near-wake vortical and wave motions has been quite well characterized (Hopfinger *et al.* 1991; Sysoeva & Chashechkin 1991; Lin *et al.* 1992; Chomaz, Bonneton & Hopfinger 1993*b*; Bonneton, Chomaz & Hopfinger 1993). The far, or late-time, wake is known to consist of patches of vertical vorticity of alternating sign that have a large horizontal extent compared with the vertical (the 'pancake' vortices). Beyond this qualitative observation, the late wake has received less attention, partly due to the experimental difficulties of modelling spatially and temporally growing structures in finite-sized facilities; most quantitative data have been single-point velocity or density time series, and in the near wake. A notable exception is the work of Chomaz *et al.* (1993*a*), who measured the velocity field at several horizontal planes in a 20 m length tow tank, and for evolution times up to $Nt = 750$.

Spedding, Browand & Fincham (1996*a,b*, referred to herein as SFB*a,b*) used a high-accuracy DPIV method, where cross-correlations of subregions of successive digital images yielded velocity distribution estimates with sufficient spatial and temporal resolution to show that the late-wake mean and turbulence profiles decayed with exponents that were similar to those found for turbulent sphere wakes in unstratified homogeneous fluids. It was also found that the peak defect velocity was up to an order of magnitude larger. The energetic mean wake flow was attributed to the high degree of order found in the arrangement of the wake vortices, which maintained a coherent structure and organization for much longer than if there were no buoyancy effects. The principal results were found to hold for all $F \in [1, 30]$. SBF*b* further demonstrated that the wake vortices themselves showed the same F-independence as did the wake-averaged quantities, and a possible three-dimensional vortex model was presented.

1.2. *Remaining puzzles*

The results of SBF*a,b* lead directly to some unanswered questions. First, it cannot always be true that the kinetic energy decay rate is the same as for a turbulent wake in a homogeneous fluid, while at the same time, the wake defect velocity magnitude is significantly higher. The existence of the latter requires the previous existence of another regime with significantly different (lower) decay rates. Second, presumably there must exist some F where the peculiar results are no longer obtained: as $F \to \infty$ we must recover the unstratified classical turbulent sphere wake, and so the reported F-independence cannot be true over all F.

1.3. *A high-Froude-number limit?*

A simple physical argument for the existence of a critical Froude number beyond which coherent wake vortices will not be observed can be made as follows: if the turbulent dissipation of the larger coherent structures (i.e. those that are responsible for the pattern geometry on scales comparable to the sphere diameter, D) occurs

on timescales that are short compared with a timescale for wake collapse, and the beginning of significant influence of buoyancy effects, then pancake vortices may never be formed, and no such structure will be visible in the far wake, which will contain only remnants of disorganized turbulent motions. The balance between the two timescales is actually an internal Froude number, which can be derived as follows.

Suppose a turbulent eddy loses a substantial fraction of its kinetic energy during one turnover time, $t_e \sim l/u$, where l is an integral length scale, and u is a characteristic turbulent velocity. Suppose also that the early wake is unaffected by stratification, in which case the turbulent length and velocity scales can be related to the sphere diameter and tow speed roughly as $l/D \simeq 0.4$, and $u/U \simeq 0.3$ (Gibson, Chen & Lin 1968; Uberoi & Freymuth 1970; Bevilaqua & Lykoudis 1978) then,

$$t_e \sim \frac{l}{u} \approx \frac{4}{3}\left(\frac{D}{U}\right).$$

Previous experiments on turbulence in stratified fluids (Browand, Guyomar & Yoon 1987; Hopfinger *et al.* 1991) indicate that the turbulence first feels the effect of stratification at $Nt = 2$–3. A buoyancy timescale is then

$$t_b \sim N^{-1} \approx \frac{2.5}{N}.$$

Inhibition of late-wake vortex formation occurs when $t_e < t_b$, and so

$$\frac{4}{3}\left(\frac{D}{U}\right) < \frac{2.5}{N},$$

or

$$\frac{2U}{ND} \equiv F > \frac{8}{7.5} \simeq 1. \tag{1.1}$$

The argument is rather simple, and precise numerical values for the coefficients should not be taken overly seriously. $F_{crit} = 1$ is obviously incorrect since numerous studies, including ours, have shown vortex wakes for F up to 30. But the underlying physical basis seems reasonable enough, and it is similar in principle to the one given by Pao, Lai & Schemm (1982), who derived a value $F_{crit} = 160/\pi$. They reported seeing no vortex wakes when $F \geqslant 300/\pi$. Both of these F values exceed most of those achieved in other experiments (varying definitions of N and F coexist in the literature; here N is in units of rad s^{-1}, and F is based on the sphere radius, $D/2$), and the notable results of SBF*a,b* (i.e. those outlined in the final paragraph of §1.1) may not be found at such high F.

However, it should also be noted that if quasi-two-dimensional wake formation occurs at a characteristic Nt_{Q2D} =const., since $x/D = Ut/D$, then the associated downstream location is

$$\left(\frac{x}{D}\right)_{Q2D} = Nt.F/2,$$

which increases with increasing F. At very high F, the wake will form many diameters behind the body, and special experimental conditions must prevail for this to be both possible and observable.

1.4. *When, and how, are stratified wakes formed?*

The principal objective is to determine whether coherent vortex wakes are formed at high Froude number. If they are not, then a critical value of F might be identifiable, separating regimes that generate persistent wakes from those that do

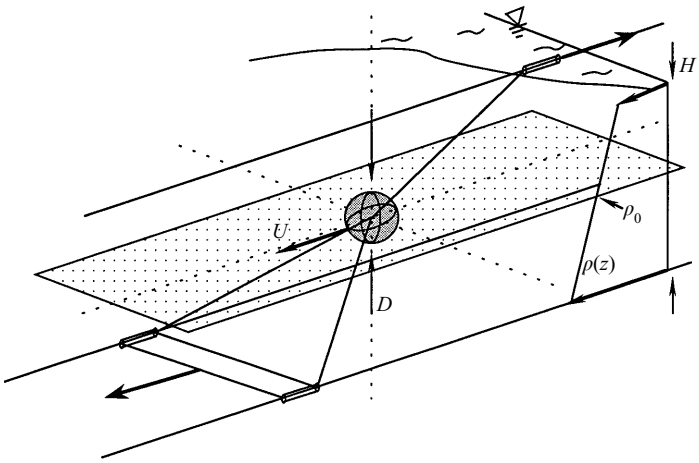

FIGURE 1. The sphere towing mechanism, and geometric parameters in the experiment. Sidewall boundaries are 1.2 m from the centreline. The total water depth, H, is 24 cm, and with the spheres in table 1, the maximum value of D/H is approximately 0.11.

not. The unusually high wake defect velocities measured by SBF*a,b* are caused by the relatively regular arrangement of wake vortices, and so would also disappear if the wake coherence is destroyed. In cases where coherent late wakes are formed, the defect magnitudes and decay rates combined imply the presence of an earlier regime with low kinetic energy decay rates. Incremental improvements and reconfiguration of the experimental methods allow velocity fields to be measured with reasonable accuracy at earlier times than before, and the second main objective is to search for evidence of this postulated transitional regime. Although the wakes comprise an interesting combination of wave and vortex motions, especially at early times, the wave components are ignored here, and all reported measurements are from the wake centreplane, where the vertical component of vorticity is strongest.

2. Experiments and analysis

2.1. *Experimental methods*

The materials and methods are similar to those described in some detail in SBF*b*. A sphere is mounted obliquely on three thin ($d = 0.025$ cm) wires connected to high-tension tow cables on the floor of the tank and just beneath the water surface (figure 1) of a 2.44×2.44 m tank. High Froude numbers are obtained primarily through a combination of high forward speed, U, and small D. The variation in these parameters, and the resulting values of F and Re for the experiments reported here are given in table 1. Re varies between 5×10^3 and 1.2×10^4, and all experiments can be considered to belong to a moderately high-Re regime where variations in Re have no measurable effect on the wake structure or its decay, as determined in SBF*b*.

At the higher tow speeds, the initial Re_d can be around 200, and so vortex shedding will certainly occur behind the support wires. Limited experiments with much smaller tracer particles ($d_p \approx 50$ μm) in a plane 3 cm above the midplane revealed a small-scale wake, but no trace of it (perturbations with a similar magnitude and length scale) could be found at the centreplane of measurement, which is not intersected by the support wires, and where these disturbances would in any case be very small compared with the wake flow.

	Exp.# ($F.Re$)	N (rad s^{-1})	D (cm)	U (cm s^{-1})	Re ($\times 10^3$)	F
♠	F10.5	1.64	2.54	20.3	5.1	10
	F20.6	1.64	1.91	30.6	5.8	20
	F40.5	1.21	1.50	36.0	5.4	40
♠	F80.10	1.63	1.27	81.3	10.3	80
	F120.12	1.21	1.27	91.4	11.6	120
♠	F160.5	1.62	0.61	77.4	4.7	160
	F200.6	1.62	0.61	96.8	5.8	200
♠	F240.5	1.21	0.61	87.1	5.3	240

TABLE 1. Experimentally realizable range of $\{N, D, U\}$ that generates a series of experiments with increasing F, and high Re. Experiments marked with a ♠ appear in figure 2.

From table 1, D/H varies between 0.106 and 0.025, and as D tends to decrease with increasing F, there is some danger of confinement effects being confused with Froude number dependence. However, since one of the most notable results is an absence of F-dependence, and a collapse of late-wake data regardless of initial F, there is no evidence to support a systematic effect of varying D/H. When only D varies, and U and N are varied to maintain a constant F at sufficiently high Re, no D/H-dependence can be detected. Observing no finite-depth effects in these particular measurements is not to say that there are none; it is easy to show, for example that the lee waves are very quickly modified by the presence of the top and bottom boundaries. However, the statistics of the motions induced by the vertical component of vorticity in the centreplane, which are the sole focus of attention here, do not appear to be affected.

The tracer particles are polystyrene beads, with a mean diameter of 600–800 μm, and a relative density, $\rho_0 = 1.0470 \pm 0.00025$, and they therefore mark an isopycnal within the specified range. At late times, vertical velocities are very small, and the isopycnal is almost a horizontal plane. Two Panasonic GP-MF552 CCD cameras record the particle motions and analog video is digitized directly into PC RAM. The recorded areas, $\{\Delta x, \Delta y\}$ under the two cameras are 71.6×54.4 cm and 145.9×111.1 cm. The factor of two difference in spatial resolution permits simultaneous measurement of different scales of motion, and provides a check on potential sampling errors when small-scale motions occur on scales comparable to, or smaller than the sampling grid.

The fields of view from the two cameras are smaller than in previous experiments, and the spatial resolution is correspondingly increased by about 25%. The camera sync signals are driven by two video frame-grabber boards operating in master-slave configuration so that one crystal oscillator controls the timing for both cameras and both video interfaces. The video phase-locking error described in SBF*b* is thus eliminated, and the bandwidth of measurable values of $\partial u/\partial y$ and $\partial v/\partial y$ is greatly increased.

2.2. *Estimation of the velocity field*

The correlation image velocimetry (CIV) technique (Fincham & Spedding 1996) is used to estimate the velocity field, and in the absence of the video phase-locking error, the error in this measurement is governed mostly by correlation peak location

accuracy, and by vertical out-of-plane motions in the fluid. The former contribution depends on the software algorithm, and can be maintained at acceptably low values. At early times, when the fluid motion in the wake is fully turbulent, and three-dimensional, the latter error predominates and no measurements are possible; this sets the earliest time (in Nt, or x/D) when the measurement can be relied upon to give a result. Aliasing errors further restrict this time, and can be checked with the two-camera system. In the results reported here, the further criterion that the characteristic wake half-width (defined below) must exceed 2 grid points ($L_\sigma > 2\Delta y$) is imposed.

2.3. *Instantaneous and mean flow-field measurements*

When the above sampling criteria are satisfied, the isopycnal surface containing the beads is very nearly flat, and the projected pattern displacements onto the measurement plane are reasonable estimates of the $\{u, v\}$ velocity components in $\{x, y\}$ (the sphere moves from right to left, in $-x$). Denoting $\boldsymbol{q} = \{u, v\}$, it is convenient to separate $\boldsymbol{q}$ into two components,

$$\left.\begin{aligned} \boldsymbol{\omega}_z &= \nabla \times \boldsymbol{q}, \\ \Delta_z &= \nabla \cdot \boldsymbol{q}, \end{aligned}\right\} \tag{2.1}$$

and the magnitudes of the vertical vorticity, $\boldsymbol{\omega}_z$, and of the divergence of the velocity field in the $\{x, y\}$-plane, Δ_z, can be regarded as approximately proportional to the amplitudes of vortex and wave motions, respectively, in a plane of constant z. Streamwise-averaged velocity profiles, $U_X(y)$ can be taken where U_X at each y is the mean value of u over the observation window length in x, Δx. When a Gaussian fit can be made of these profiles, $U_X(y)$ can be described by

$$U_X(y) = U_0 \mathrm{e}^{-(y/L_\sigma)^2/2},$$

and L_σ is a measure of the wake half-width. More generally, the wake region is defined as the horizontal band in y where $U_X(y) > 0.2U_0$, and U_0 is the maximum of $U_X(y)$ over Δy. Wake-averaged values are denoted by $\langle\rangle$ and are taken over this wake region. The measurable components of the kinetic energy, enstrophy and dissipation are

$$\left.\begin{aligned} E &= \tfrac{1}{2}\langle u^2 + v^2 \rangle, \\ W &= \tfrac{1}{2}\langle \omega_z^2 \rangle, \\ S &= 2\nu \langle s_{ij} s_{ij} \rangle, \end{aligned}\right\} \tag{2.2}$$

respectively, where the rate-of-strain tensor, s_{ij}, is summed over x and y. The wake measurements can be plotted as a function of evolution time as Nt, or since $x/D = (F/2)Nt$, as an equivalent downstream distance, x/D.

3. Results

3.1. *Vertical vorticity field in the late wake*

Figure 2(*a,b*) shows four time series of the vertical vorticity field for values of F ranging from 10 to 240. It is immediately obvious that coherent, well-ordered vortex wakes are generated in all cases. The coherent structures are quite well-established by $Nt \approx 50$, and reduce their number (per observation box) by pairing interactions thereafter. The time of the right-hand column of figure 2(*a*) is repeated in the left column of figure 2(*b*), which continues the time series with the wide-angle camera.

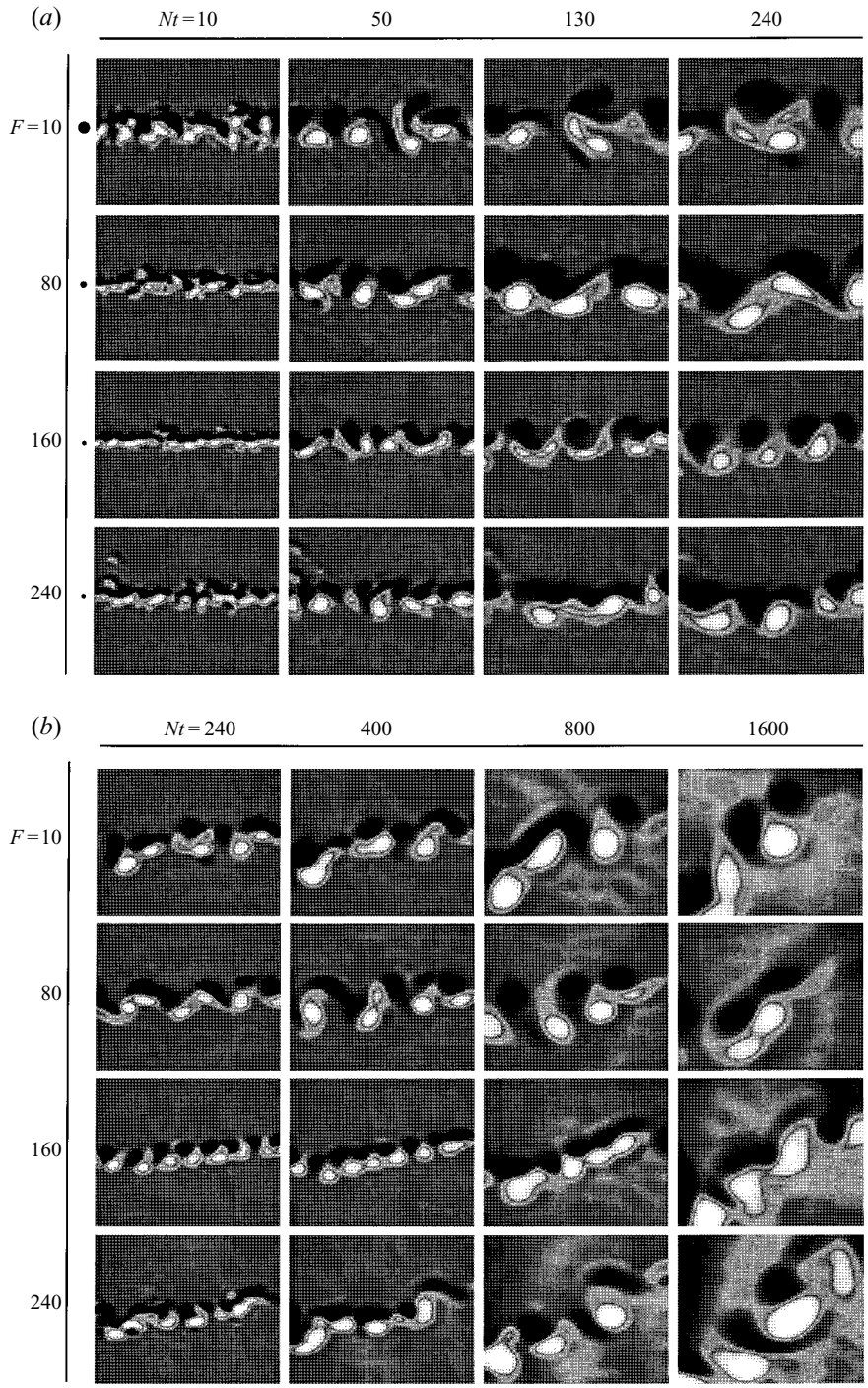

FIGURE 2. $\omega_z(x, y, Nt)$ for $F = \{10, 80, 160, 240\}$. In (*a*), the image area, $\{\Delta x, \Delta y\} = 72 \times 54$ cm. The relative sphere sizes are shown by dark circles in the left margin. The time $Nt = 240$ is repeated in (*b*) where $\{\Delta x, \Delta y\} = 146 \times 111$ cm. At $t = 0$, the sphere was at $\Delta x/2$, moving from right to left. The colour bar is rescaled symmetrically about $\omega_z = 0$ to the local maximum value of $|\omega_z|$ at each timestep. The vertical and horizontal background patches are interference patterns from scanning and reduction of the digital images, and are not related to the data.

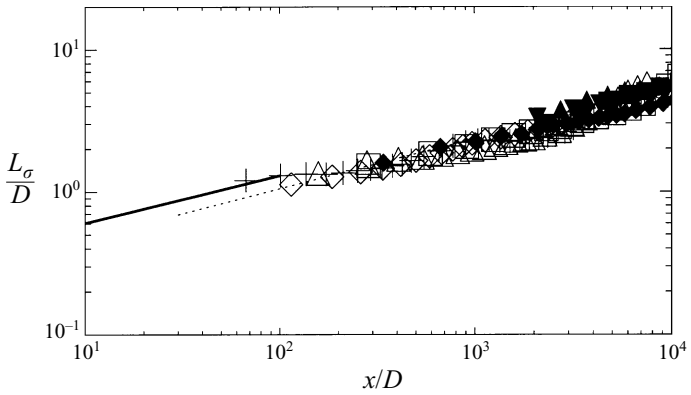

FIGURE 3. The sphere wake half-width, L_σ/D *vs.* downstream distance, x/D, for $F = \{10, 20, 40, 80, 120, 160, 200, 240\}$, denoted by symbols $\{+, \diamond, \triangle, \square, \blacklozenge, \blacktriangle, \blacksquare, \blacktriangledown\}$. The solid line is experimental data for an unstratified, turbulent sphere wake (Bevilaqua & Lykoudis 1978). The dotted line is from SBF*b* for $F \in [1, 15]$.

At large Nt, a mean rotation of the vortex wake can be seen, due to the presence of a background tank-scale vortical motion. Although it complicates the analysis of the wake geometry somewhat, the background vorticity is at least four orders of magnitude weaker than the wake vortices themselves, and the effect is treated as a simple superposition of the wake on a mean background flow. Other than the mean rotation, by $Nt = 1600$ in the right-hand column of figure 2(*b*) the wake structure is still clearly identifiable and the vortices have not drifted far from each other. If there is a high-Froude-number limit on the formation of the coherent wake vortices, then it has not been reached by $F = 240$.

3.2. *Power laws for stratified wakes at intermediate and large Nt*

3.2.1. *Mean flow*

The wake-averaged half-width, L_σ, shows a $1/3$ power law increase with x/D, from $x/D = 100$ up to 10000, for all values of F from 10 to 240 (figure 3). The curves collapse both on the previously reported high-Re data from SBF*a,b*, and on the solid line from turbulent sphere wakes in a homogeneous fluid. At first sight, the similarity of the high-F data with the three-dimensional result is unremarkable, but it is notable that the power law evolution is adhered to for such large x/D (it is not very clear that unstratified turbulent wakes ought necessarily to show such a decay law so far downstream either). Moreover, when local values of F and Re are low, and the flow field is quasi-two-dimensional in that the vertical velocities are almost zero, the similar $1/3$ growth in the $\{x, y\}$-plane cannot be attributed to similar physical mechanisms.

The downstream evolution of the mean centreline velocity (figure 4*a*), by contrast, differs significantly from previous results, and shows a systematic variation with F. As soon as reliable measurements can be made, the initial centreline velocity lies below that previously reported for wakes with $F \in [1, 10]$ (upper dotted line). At any x/D, the degree of departure is proportional to F; very high-F wakes have initial values that are close to three-dimensional wakes. Yet, with increasing x/D, the wake defect eventually becomes similar in magnitude to the lower-F cases, because intermediate decay rates ($\sim (x/D)^{-0.25\pm0.05}$) are much lower than the eventual values $\sim (x/D)^{-0.76}$. Ultimately, at some x/D whose value increases with increasing F, the stratified wakes

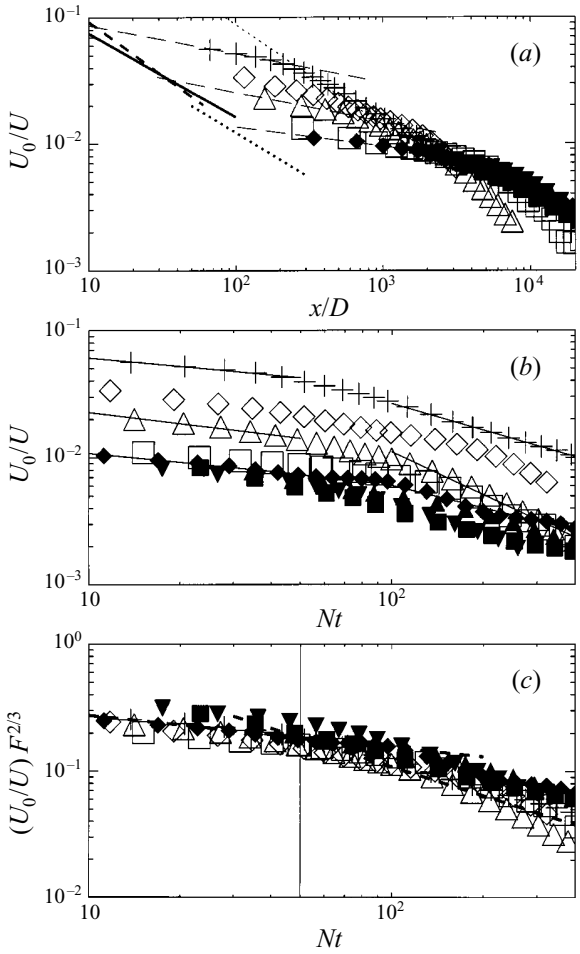

FIGURE 4. (*a*) The wake-averaged defect velocity, U_0/U *vs.* x/D, for the same cases and symbols as figure 3. Unstratified wake data: ——, Bevilaqua & Lykoudis (1978); – – –, Gibson *et al.* (1968); · · · ·, Uberoi & Freymuth (1970). The thin dotted line is from SBF*b*. The thin dashed lines are least-squares fits to the initial data for $F = \{10, 40, 120\}$. (*b*) Same data as (*a*), replotted *vs.* Nt. The limit in Nt is $Nt = 400$ because at larger values individual wakes can become distorted by tank-scale background motions. It is possible to make two sets of linear fits on each curve, before and after a corner point that occurs between $Nt = 40$ and 100. (*c*) The data collapse when appropriately normalized with F. Mean least-square fits are shown by dashed lines, which intersect at $Nt_{II} \approx 50$.

result is recovered, and all curves collapse (within experimental uncertainty, with some scatter at large x/D).

The initial power-law fit for the low decay rate regime can be extrapolated backwards in x/D to find intersections with the three-dimensional results (thick solid lines in the upper left of figure 4*a*). Similarly, the fit can be extrapolated forward (increasing x/D) to locate an intersection with the stratified wakes result of SBF*a,b*, which also appears to be an asymptotic result for the high-F wakes at large x/D. Three examples for $F = 10$, 40, 120 are shown with dashed lines in figure 4 (*a*). The intersection location in x/D can be converted back to units of Nt, and while the x/D value of both intersections varies greatly with F, they occur at approximately constant values of Nt, with no systematic variation with F for $F \in [10, 240]$. Denoting

the dimensionless time at which an initially three-dimensional turbulent wake result would depart from the data established for unstratified fluids as Nt_I, and the point at which the intermediate wake decay approaches the stratified wake result as Nt_{II}, empirical values for these characteristic times are

$$Nt_I = 1.7 \pm 0.3,$$

and

$$Nt_{II} = 50 \pm 15.$$

It is interesting to note that $Nt_{II} = 50$ coincides with the approximate time at which a qualitative similarity and degree of order and regularity of the wakes in figure 2 has already been remarked upon. That is also consistent with the attribution of the high defect velocities to the high degree of structure in the vertical vorticity field.

If characteristic breaks in the centreline velocity occur at constant Nt, then similar points ought to line up when Nt is plotted on the abscissa, which is exactly what happens in figure 4(*b*). The magnitude of U/U_0 clearly depends on F in a systematic way. Although the variability increases at the higher F values (probably a consequence of extra disturbances caused by the high towing speeds, see table 1), it seems reasonable to draw two straight line fits, one before and one after Nt_{II}. This was done for $10 \leqslant Nt \leqslant 35$ and $100 \leqslant Nt \leqslant 400$, respectively. If the defect velocity power law decay is $U/U_0 \sim (Nt)^{\alpha}$, then the two decay rates are

$$\alpha_I = -0.25 \pm 0.04,$$

and

$$\alpha_{II} = -0.76 \pm 0.12.$$

α_{II} does not differ significantly from either the previously reported stratified wakes result of -0.75 from SBF*b*, or from the $-2/3$ result expected in an unstratified turbulent wake. The α_I result differs significantly from both. Neither of these empirical constants varies with F for $F \in [10, 240]$.

At high Froude numbers, the wake might be expected to develop, at least initially, much the same as a three-dimensional wake, where one expects

$$U/U_0 \sim (x/D)^{-2/3}.$$

The appropriate form in terms of Nt is then

$$(U/U_0)F^{2/3} \sim (Nt)^{-2/3}. \tag{3.1}$$

Figure 4(*c*) shows that (3.1) collapses all the high-F data with moderate success. Although there is some indication that the higher-F range (in solid symbols) consistently lies above the lower-F data, no systematic trend can be found with F, and the differences do not exceed the experimental uncertainty. Straight lines have been drawn either side of Nt_{II} representing the mean least-squares fit over all values of F from 10 to 240. Empirical values for numerical constants in (3.1) written as $(U/U_0)F^{2/3} \simeq C_0(Nt)^{C_1}$, are given in table 2. The lines intersect at $Nt_{II} \approx 50$, as indicated by the thin vertical line in figure 4(*c*). The low slope of the initial data before Nt_{II} indicates commensurately lower kinetic energy decay rates during this time.

Subsequently, all stratified wakes asymptote to a line that characterizes the decay rate for a wake in the presence of non-zero background density gradient. The decay rate then increases, and, fortuitously, takes on a value that is indistinguishable from that of an unstratified wake. Thanks to the preceding stage though, the

Time	C_0	σ_{C_0}	C_1	σ_{C_1}
$Nt < Nt_{II}$	0.5	0.1	−0.25	0.04
$Nt > Nt_{II}$	3.6	1.9	−0.76	0.12

TABLE 2. Empirical constants for the mean wake centreline velocity decay for intermediate ($< Nt_{II}$) and late ($> Nt_{II}$) wakes.

velocity defect magnitudes will always be higher. There is no indication that the higher-Froude-number wakes behave any differently in this respect than the lower-Froude-number ones; the observed transitions to the long-time power laws simply occur at progressively higher values of x/D.

3.2.2. *Turbulence quantities*

In the light of the constant values of Nt_I, Nt_{II} observed in the mean velocity profiles, the turbulence quantities can also usefully be expressed in stratification parameters, and the normalized wake-averaged velocity fluctuation magnitude, $E^{1/2}$, vorticity magnitude, $W^{1/2}$, and the kinetic energy dissipation rate, S, and their predicted decay rates with Nt are

$$\left.\begin{aligned} \left(\frac{E^{1/2}}{U}\right) F^{2/3} &\sim (Nt)^{-2/3}, \\ \left(\frac{W^{1/2}}{U/D}\right) F &\sim (Nt)^{-1}, \\ \left(\frac{S}{U^3/D}\right) F^{7/3} &\sim (Nt)^{-7/3}. \end{aligned}\right\} \tag{3.2}$$

It is perhaps worth restating the assumptions behind writing the equations in this form. They arise from a simple substitution of Nt into relations that originally describe turbulent wakes in a homogeneous fluid. The appearance of F in the left-hand side is balanced by the power of Nt in the right-hand side, which is akin to assuming that F plays no role, as might be argued to be the case for high-F wakes at early times, where the influence of the background stratification is not yet felt. Lin & Pao (1979) followed a similar procedure in collapsing data for self-propelled slender bodies for $Nt \leqslant 60$ and $F \in [7, 180]$. Somewhat more surprising was the result of SBF*b* that these kinds of scalings collapsed the data for Nt up to 1000, $F \in [1, 10]$.

Figure 5(*a–c*) shows that the rescaled wake-averaged energy, enstrophy and dissipation measures collapse quite well for all $F \in [20, 240]$. The magnitude and decay rates of all quantities are not different from those reported in SBF*b* for $F \in [1, 10]$ at late times, but both $E^{1/2}$ and $W^{1/2}$ (figure 5*a,b*) show lower initial decay rates, up until $Nt \approx 50$, which is the same value as Nt_{II} identified in the mean profile data. By contrast, the wake-averaged dissipation rate, S, shows no such breakpoint, and continues with more or less the same power-law behaviour, right through the critical value of Nt_{II} (albeit with some scatter). On a practical level, it is reassuring that the velocity gradients contributing to S show no roll-off at early times, because it demonstrates that the roll-off in the other quantities is not likely to be due to resolution problems in the measurement. From the fluid dynamics point of view, it is clear that S is not strongly connected with the actual total kinetic energy decay.

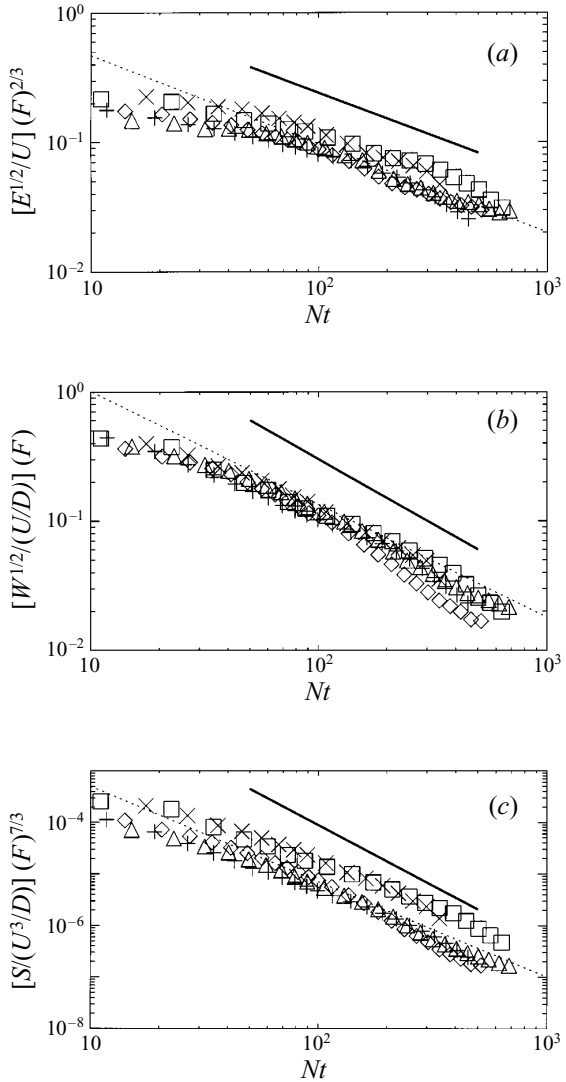

FIGURE 5. The evolution of wake-averaged turbulence quantities; (*a*) fluctuating velocity, (*b*) vorticity magnitude and (*c*) energy dissipation rate, renormalized with stratification parameters, for $F = \{20, 40, 80, 160, 240\}$, with symbols $\{+, \diamond, \triangle, \square, \times\}$. The dotted line shows the least-squares fit from previous experiments of SBF*b* for $F \in [1, 30]$, and the solid line indicates the range of Nt where the fit was calculated.

Alternative physical mechanisms must therefore be advanced to account for the low decay rates observed at early times.

The quantities $E^{1/2}$ and $W^{1/2}$ continue to be measurable above the background noise, extrapolated to $Nt \approx 1000$, as shown in the figure 6, from the highest-Froude-number experiment, $F = 240$. The late-time decay rates are not significantly different from the -0.76 and -1 values of SBF*b* for $F \leqslant 10$. Although conservative assumptions were made in calculating and extrapolating these data, it is obvious from figure 2 (bottom line) that the vortex structure is recognizable and so detectable up to $Nt = 1600$, and beyond.

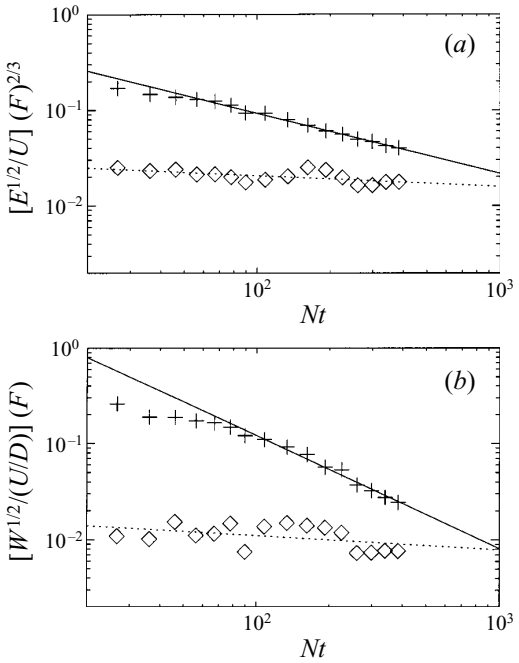

FIGURE 6. The interior (+) wake-averaged fluctuation velocity magnitude (*a*), and vertical vorticity magnitude (*b*), compared with the background levels ($\diamond$) for $F = 240, Re = 5.3 \times 10^3$. The solid lines were fit over the Nt range 80–400, and have slopes −0.63 and −1.17, respectively.

4. Discussion

4.1. *All stratified towed-sphere wakes develop coherent vortices*

Figure 2 demonstrates that coherent wake vortices are formed even at high F, without any sign of a critical value of F. By $Nt = 50$, the basic structure has emerged, and further changes in the number of vortices can be associated with specific merging events. As in previous work, it is notable that isolated couples (composed of pairs of opposite-signed vortices) do not form and propagate far from the wake centreline, but rather appear to participate in some global wake structure. The patches of vertical vorticity persist as identifiable patterns in the centreplane up until $Nt = 1600$, and beyond. Neither of these properties seems to vary with F for $F \in [10, 240]$, a result that was also reported by SBF*b* for $F \in [1, 30]$.

Chomaz *et al.* (1993*b*) identified the strongest periodic component of the near stratified wake as a collapsed spiral instability mode, the stratified equivalent of the global helical instability that Monkewitz (1988) suggested can be driven by a self-excited oscillation in the near wake when $Re > 3.3 \times 10^3$. SBF*b* found a minimum $Re \approx 4 \times 10^3$ for self-similar late-wake scaling for $F \in [1, 30]$. Given the same minimum Re, reasonable similarity is found here for all $F \geqslant 10$. The late-wake Strouhal number is not the same as the initial helical mode because merging of like-signed vortices occurs in each dynamically connected layer. However, the pattern and topology of the residual vortex motions in the late wake preserves information concerning the initial generating conditions – in this case, the helical instability mode.

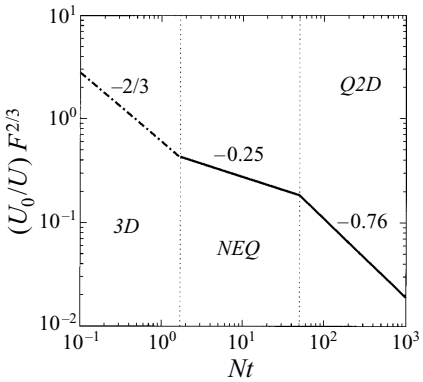

FIGURE 7. A universal curve for the evolution of decaying turbulent wakes in a stably stratified fluid. Three regimes can be identified: a three-dimensional turbulent initial wake, a transitional, non-equilibrium regime (*NEQ*) where wake collapse occurs and low kinetic energy decay rates in the plane are accompanied by conversion of potential to kinetic energy, and finally, a quasi-two-dimensional (*Q2D*) state where vertical motions have all but ceased. The *NEQ* and *Q2D* curves were measured, and the constants C_0 and C_1 in $(U/U_0)F^{2/3} \simeq C_0(Nt)^{C_1}$ for the two regions are from table 2. If $C_1 = -2/3$ in the three-dimensional regime, then intersection at Nt_I requires $C_0 \simeq 0.6$. The vertical dotted lines mark constant transitional values of $Nt_I \approx 2$ and $Nt_{II} \approx 50$.

4.2. *The transition from turbulence to pancakes*

4.2.1. *Universal scaling in stratified wakes*

If the constant power-law extrapolation back to a three-dimensional turbulent flow regime is valid, then the discovery of two characteristic times, Nt_I and Nt_{II}, that separate dynamically similar regions, together with the collapse of data in figure 4(*c*), suggests that a general curve for all stratified drag wakes can be constructed, and such a curve is shown in figure 7. The solid lines are drawn from the constants in table 2, and the dashed line is deduced from intersections of the data at Nt_I. The early- and late-wake regions, labelled *3D* and *Q2D*, respectively, are separated by a region with significantly lower decay rates of energy (and enstrophy). Physically, it corresponds to an adjustment, or non-equilibrium (*NEQ*) period, when potential energy of vertically displaced fluid is partly reconverted back to kinetic energy close to the wake centreline. Figure 5(*c*) shows that the time evolution of the measurable turbulent dissipation, S, does not change during this period; rather it is the increased production from buoyancy that leads to the reduced decay rates of turbulent kinetic energy and enstrophy, E and W, in figure 5(*a,b*). The low decay rates associated with the *NEQ* regime are responsible for the relatively high wake energy during the *Q2D* phase, as previously reported in SBF*b*.

Certain features of figure 7 are quite well-supported by existing data in the literature. Browand *et al.* (1987) and Hopfinger (1987) review previous work and report $Nt = 1$–2 as being the time at which turbulence first feels the effect of the ambient stratification. Lin & Pao (1979) showed the occurrence of the first maximum wake height of a self-propelled slender body at a constant value of $Nt_c = 1.4$ for $F \in [20, 180]$, and $Nt_c = 4.7$ for towed slender bodies for $F \in [10, 110]$. Itsweire, Helland & Van Atta (1986) found a maximum overturning scale at $Nt \approx 1.5$–1.7 for spatially decaying grid turbulence in a salt-stratified water channel. Hopfinger *et al.* (1991) reported that wake growth for a towed sphere at moderate Froude number ($F \geqslant 4$) was initially affected by stratification at around $Nt = 2$. Xu, Fernando & Boyer (1995) found that the maximum wake height behind a towed cylinder occurs at $Nt \approx 2.5$ for $F > 3$.

The value of $Nt_I = 1.7$ estimated here, and the fact that it is constant for reasonably high initial Froude numbers seems to be consistent with these numbers.

The low decay rates in the *NEQ* regime derive from the conversion of potential to kinetic energy, and will be associated with negative buoyancy flux ($B = \overline{\rho w}/\rho' w'$) as the turbulence collapses, and restratification occurs. Lin & Pao (1979) reported slower decay rates of the r.m.s. longitudinal velocity fluctuations in the wake of a self-propelled, slender body for $Nt \geqslant 18$. A significantly reduced decay rate in the vortical mode, associated with turbulent collapse, was reported by Métais & Herring (1989) at $Nt \approx 6$ for numerical calculations of freely decaying stratified turbulence. They also found negative periods in oscillatory buoyancy fluxes for $Nt = 2$–6.5, in broad agreement with the experimental measurement of $B < 0$ for $Nt = 2$–10 by Itsweire *et al.* (1986). The observed reduction in decay rates of energy and enstrophy during intermediate times is consistent with the proposed dynamics of the *NEQ* regime in figure 7. It is likely that all freely decaying stratified flows, at sufficient $\{Re, F\}$, will have such a regime.

The point at which the *NEQ* flow transitions to a *Q2D* regime is denoted as $Nt_{II} \approx 50$ and does not depend on F for the towed-sphere wake. However, Browand *et al.* (1987) give the formation time of intrusions behind an oscillating grid as $Nt \approx 10$, noting that it occurs well after the time at which the turbulence is first affected (Nt_I here). Similarly, Hopfinger *et al.* (1991) find that the spiral mode in the near wake for $F \geqslant 4$ can be distinguished up until $Nt = 3.4$, that overturning of progressively smaller eddies can be seen up to $Nt \approx 9$, with a fully collapsed far-field wake appearing at $Nt \approx 20$. Métais & Herring (1989) showed a variation in the relative magnitude of w and $\boldsymbol{q}$ at $Nt \approx 25$ according to initial conditions, but the velocity field in the $\{x, z\}$-plane that evolved from predominantly vortical mode initial conditions showed strong evidence of layered motions at this time. In Fincham, Maxworthy & Spedding (1996), layer formation can be seen by $Nt \approx 180$. Nt_{II} thus does not appear to be constant for different experiments. Perhaps it is unsurprising that the late-time dynamics of physical processes that have a memory of their initial conditions do not have a universal start time (Nt_{II}), while Nt_I, involving the modification of a fully developed turbulence, does have a fixed value.

4.2.2. *The time evolution of a stratified wake*

Tracing the curve of figure 7, the following sequence of events takes place: initially, during the *3D* phase, the turbulent wake is unaffected by stratification, and decays as a three-dimensional wake. At $Nt \approx 2$ the kinetic energy is no longer sufficient to sustain motions that would lift fluid parcels from their equilibrium position over scales that are comparable to the average turbulent eddy size. Some fluid elements that have been displaced from their neutral position relax back, converting their stored potential energy to kinetic energy. The 'relaxation' process continues during the non-equilibrium (*NEQ*) regime from the collapse of previous vertical excursions. Some energy is propagated away as internal waves, while some is returned to the remaining wake, which is increasingly confined to a region of small vertical extent about the centreplane. The energy density here decreases much more slowly than usual (in the absence of stratification), and the overall decay rates of kinetic energy and enstrophy in the centreplane are low. Turbulent dissipation mechanisms proceed, and much random small-scale structure is lost. What remains are contiguous patches of vertical vorticity, whose structure is related to the original wake instability, as discussed in the previous section.

There is a close correspondence between the *NEQ* and *Q2D* regimes and the

fossil-turbulence model of Gibson (e.g. 1986), and the time evolution of the $3D \rightarrow NEQ \rightarrow Q2D$ path follows the trajectory of a solution through active, active-fossil, and fossil states in a hydrodynamic phase diagram (see Gibson 1991). However, since data concerning vertical lengthscales and contributions to ϵ from vertical shearing (noting only that they are likely to be an order of magnitude greater than ϵ_z) are lacking, it is perhaps prudent to defer further conjecture that requires or presumes this information. In particular, it should be noted that data such as figure 2 do not show motionless remnants of previous events, but rather are measures of current vortical motions. Lengthscales in the horizontal and vertical are highly anisotropic, and the dynamics can hardly be described as turbulent, in the usual sense, as indeed Gibson (1986, 1991) has taken some pains to point out.

Closely related experiments on decaying stratified grid turbulence (Fincham *et al.* 1996) suggest that the end of the *NEQ* phase is accompanied by the formation of multiple layers separated by sheets of strong horizontal vorticity. The vertical shearing motions are responsible for almost all of the dissipation, as also found in certain of the numerical simulations of Métais & Herring (1989). At the end of the *NEQ* regime, the basic late-wake vortex structure (as modelled by SBF*b*) is established. The characteristic time is $Nt_{II} \approx 50$ for the particular case of towed-sphere wakes. Although vertical shear instabilities can still occur, the vertical velocity, w, approaches zero during the early part of the *Q2D* regime, after which the flow within each layer proceeds, almost as if unaffected by stratification, except in the vertical shearing between adjacent (almost) horizontal layers. The combined effect is to produce decay rates that are quite similar to those in three-dimensional unstratified wakes, but the similarity is coincidental.

Although the majority of the potential-to-kinetic energy conversion occurs during the *NEQ* phase, it does not entirely cease in the *Q2D* motions that can represent a balance between buoyancy and viscous forces, as slow laminar motions accompany a return to complete restratification, as originally described by Pearson & Linden (1983). Small-scale vorticity fluctuations are removed by viscosity, and during the *Q2D* stage the remaining large-scale vortex structures represent a memory of the initial shedding mode on the sphere. Although not required to explain the persistence of regularity in the late wake, many stratified flows possess a noted capacity for emergence of orderly structures from apparently disorganized initial conditions (see, for example Voropayev & Afanasyev 1994). The ideas concerning self-organization and emergence of coherent structure in two-dimensional flows through a mamimum-entropy constraint, proposed by Robert & Sommeria (1991) and further elaborated by Chavanis & Sommeria (1996), are in part aimed specifically at regimes of geophysical interest, and their potential relevance to this problem deserves serious consideration in the future. Once formed, the *Q2D* wake structure persists up to very large Nt unless otherwise disturbed. It does so, not because the decay rates are particularly low, but because the pattern geometry is maintained during this time.

5. Concluding remarks

5.1. *Distinguishing characteristics of stratified turbulence*

There is a qualitative difference between turbulent flows that evolve in the presence of some non-zero background density gradient and those that occur in a homogeneous fluid. At sufficiently large times, or sufficiently far downstream of the original turbulent source, all freely decaying stratified turbulent flows, with arbitrarily large initial F,

eventually reach a state where the local F is small, and the dynamics are dominated by buoyancy effects. The final asymptotic state is the *Q2D* phase in figure 7. The notion advanced in §1.2, that the unstratified result will surely be recovered as $F \to \infty$, is therefore false, because all flows at finite F are different from the particular case where $F = \infty$.

Although the foregoing statements extrapolate beyond the more restricted domain of the measurements (with $F \in [1, 240]$), it is the contention here that the physical mechanisms responsible for the characteristic decaying stratified wake, and discussed further in the following two subsections, are not expected to suddenly fail at some higher F_{crit}. Instead, the more parsimonious explanation, based on available data, will continue the trend to all finite F.

5.2. *The NEQ → Q2D transition*

The postulated buoyancy-driven forcing behind the *NEQ* regime is not particular to towed bluff-body wakes, but could be expected whenever a spatially limited initially turbulent region evolves in the presence of a stable stratification. Similarly, it is proposed that all such flows will eventually reach a *Q2D* phase, where $w \approx 0$, and motions occurring in each layer are coupled vertically by high-shear regions that are responsible for most of the dissipation. Since the basic physical mechanisms are the same, then the late-time decay rates ought also to be the same. This does not include cases where forcing is uniform in the vertical, because particular mechanisms for expansion into undisturbed ambient (the enhanced vertical diffusion of Chomaz *et al.* 1993*a*), or rearrangement of vertically coupled vortex loops (SBF*b*) that are seen to occur in the wake flows may be modified. However, based on the foregoing argument, the same late-wake decay rates would be predicted for both towed and self-propelled slender bodies, even though their near-wake behaviour in the three-dimensional regime is known to be different (see Lin & Pao 1979).

5.3. *The formation of coherent vortices, and their persistence*

There is no evidence to support the notion of a high-F limit for the emergence of the pancake vortex wake structure in the wake of a towed bluff body. Persistent organized vortex wakes have been measured over all Froude numbers tested (here and SBF*b*): $F \in [1, 240]$. The range and upper limit are sufficiently high that it is unlikely that some elusive F_{crit} lies just beyond reach. Evidently, the initial turbulence does not completely disorganize itself and destroy the possibility of formation of coherent wakes. Some regularity in the initial vortex wake structure (the spiral) survives to determine the late-wake coherence. This is not so surprising since Bevilaqua & Lykoudis (1978) demonstrated a memory in unstratified turbulent sphere and disk wakes, and stratified fluids are known for their propensity for preserving information concerning initial conditions, in both laboratory and numerical experiments (e.g. Métais & Herring 1989; see also more general remarks in Hunt & Carruthers 1990). If the initial wake instability is different, then this should be reflected also in the pattern of vortex patches in the far wake, but not in the issue of their existence/non-existence. Note that the late wakes do not have especially low dissipation rates; rather it is the stability and persistence of their spatial structure that is notable. The vortex patterns live for longer than it is reasonable to run experiments, up to $Nt \approx 1600$ here, even at high F.

5.4. *Practical issues*

Froude numbers of undersea vehicles moving at medium or high speeds are likely to be in the 200–400 range, so they ought to generate long-lived vortex wakes, just like those of figure 2. The distribution of vortices in the wake of a self-propelled body is likely to be more complicated than for a towed body, because the mean wake profiles in momentumless wakes have four shear layers, rather than two (as noted by Lin & Pao). If $N \approx 2 \times 10^{-3}$ rad s^{-1} in the ocean pycnocline, then $Nt = 1600$ corresponds to $t = 8 \times 10^5$ s, or about 9 days.

The geometrical and dynamical similarity of the wake and its time evolution require some minimum Re (wakes with initial $Re < 4 \times 10^3$ did not show similar scaling in SBF*b*), but are predicted to apply to all higher-Re cases. The range of absolutely unstable Strouhal numbers for high Re (3.3×10^3 to 10^5) for helical mode shedding in Monkewitz (1988) is an asymptotic limit for $Re \rightarrow \infty$, and there is also empirical evidence that mesoscale eddy formation behind islands or mountain-sized topography occurs when Re is probably on the order of 10^{10} to 10^{11} (e.g. Pao & Kao 1976).

Another practical issue is the susceptibility of the coherent wakes to disruption from outside forcing, in particular from ambient shear. Although the wake turbulence does not appear to self-disorganize, higher-Froude-number wakes could be more prone to disturbance from external perturbations before or during the *NEQ* regime that precedes the coherent wake, because the structure emerges only a large number of body diameters, x/D, downstream. Since the real ocean or atmosphere is never perfectly homogeneous in space or in time, the F-independence may yet be a result that is peculiar to clean laboratory facilities.

I would like to thank Professor F. K. Browand for invaluable advice and suggestions that greatly improved this paper. Many thanks also to Dr Adam Fincham for vital assistance during the early stages of the experimental work. This work is funded by ONR Grant# N00014-96-1-0001, administered by Dr L. P. Purtell, whose continued, constructive support is most gratefully acknowledged.

REFERENCES

Bevilaqua, P. M. & Lykoudis, P. S. 1978 Turbulence memory in self-preserving wakes. *J. Fluid Mech.* **89**, 589–606.

Bonneton, P., Chomaz, J. M. & Hopfinger, E. J. 1993 Internal waves produced by the turbulent wake of a sphere moving horizontally in a stratified fluid. *J. Fluid Mech.* **254**, 23–40.

Browand, F. K., Guyomar, D. & Yoon, S. C. 1987 The behaviour of a turbulent front in a stratified fluid: experiments with an oscillating grid. *J. Geophys. Res.* **92**, 5329–5341.

Chavanis, P. H. & Sommeria, J. 1996 Classification of self-organized vortices in two-dimensional turbulence: the case of the bounded domain. *J. Fluid Mech.* **314**, 267–297.

Chomaz, J. M., Bonneton, P., Butet, A. & Hopfinger, E. J. 1993*a* Vertical diffusion in the far wake of a sphere moving in a stratified fluid. *Phys. Fluids* A **5**, 2799–2806.

Chomaz, J. M., Bonneton, P. & Hopfinger, E. J. 1993*b* The structure of the near wake of a sphere moving horizontally in a stratified fluid. *J. Fluid Mech.* **254**, 1–21.

Fincham, A. M., Maxworthy, T. & Spedding, G. R. 1996 Energy dissipation and vortex structure in freely-decaying, stratified grid turbulence. *Dyn. Atmos. Ocean* **23**, 155–169.

Fincham, A. M. & Spedding, G. R. 1996 Low-cost, high-resolution DPIV for turbulent flows. *Exps. Fluids* (submitted).

Gibson, C. H. 1986 Internal waves, fossil turbulence, and composite ocean microstructure spectra. *J. Fluid Mech.* **168**, 89–117.

Gibson, C. H. 1991 Laboratory, numerical, and oceanic fossil turbulence in rotating and stratified flows. *J. Geophys. Res.* **96**, 12549–12566.

Gibson, C. H., Chen, C. C. & Lin, S. C. 1968 Measurements of turbulent velocity and temperature fluctuations in the wake of a sphere. *AIAA J.* **6**, 642–649.

Hopfinger, E. J. 1987 Turbulence in stratified fluids: a review. *J. Geophys. Res.* **92**, 5287–5303.

Hopfinger, E. J., Flór, J. B., Chomaz, J. M. & Bonneton, P. 1991 Internal waves generated by a moving sphere and its wake in a stratified fluid. *Exps. Fluids* **11**, 255–261.

Hunt, J. C. R. & Carruthers, D. J. 1990 Rapid distortion theory and the 'problems' of turbulence. *J. Fluid Mech.* **212**, 497–532.

Itsweire, E. C., Helland, K. N. & Van Atta, C. W. 1986 The evolution of grid-generated turbulence in a stably stratified fluid. *J. Fluid Mech.* **162**, 299–338.

Lighthill, M. J. 1996 Internal waves and related initial-value problems. *Dyn. Atmos. Ocean* **23**, 3–17.

Lin, J. T. & Pao, Y. H. 1979 Wakes in stratified fluids: a review. *Ann. Rev. Fluid Mech.* **11**, 317–338.

Lin, Q., Lindberg, W. R., Boyer, D. L. & Fernando, H. J. S. 1992 Stratified flow past a sphere. *J. Fluid Mech.* **240**, 315–354.

Métais, O. & Herring, J. R. 1989 Numerical simulations of freely evolving turbulence in stably stratified fluids. *J. Fluid Mech.* **202**, 117–148.

Monkewitz, P. A. 1988 A note on vortex shedding by axisymmetric bluff bodies. *J. Fluid Mech.* **192**, 561–575.

Pao, H. P. & Kao, T. W. 1976 On vortex trails over ocean islands. *Atmos. Sci. J. Met. Soc. Rep. China* **3**, 28–38.

Pao, H. P., Lai, R. Y. & Schemm, C. E. 1982 Vortex trails in stratified fluids. *Johns Hopkins Technical Digest* **3**, 12–18.

Pearson, H. J. & Linden, P. F. 1983 The final stage of decay of turbulence in stably stratified fluid. *J. Fluid Mech.* **134**, 195–203.

Robert, R. & Sommeria, J. 1991 Statistical equilibrium states for two-dimensional flows. *J. Fluid Mech.* **229**, 291–310.

Spedding, G. R., Browand, F. K. & Fincham, A. M. 1996*a* The long-time evolution of the initially-turbulent wake of a sphere in a stable stratification. *Dyn. Atmos. Ocean* **23**, 171–182 (referred to herein as SFB*a*).

Spedding, G. R., Browand, F. K. & Fincham, A. M. 1996*b* Turbulence, similarity scaling and vortex geometry in the wake of a sphere in a stably-stratified fluid. *J. Fluid Mech.* **314**, 53–103 (referred to herein as SFB*b*).

Sysoeva, E. Y. & Chashechkin, Y. D. 1991 Vortex systems in the stratified wake of a sphere. *Izv. Akad. Nauk SSSR, Mekh. Zhidk. Gaza* **4**, 82–90.

Uberoi, M. S. & Freymuth, P. 1970 Turbulent energy balance and spectra of the axisymmetric wake. *Phys. Fluids* **13**, 2205–2210.

Voropayev, S. I. & Afanasyev, Y. D. 1994 *Vortex Structures in a Stratified Fluid*. Chapman & Hall.

Xu, Y., Fernando, H. J. S. & Boyer, D. L. 1995 Turbulent wakes of stratified flow past a cylinder. *Phys. Fluids* **7**, 2243–2255.